Vasishta Ganguly
Research Assistant
e-mail: vganguly@uncc.edu

Tony Schmitz
Associate Professor
e-mail: tony.schmitz@uncc.edu

Department of Mechanical Engineering
and Engineering Science,
University of North Carolina at Charlotte,
Charlotte, NC 28262

Arthur Graziano
Research Assistant
e-mail: graziano@ufl.edu

Hitomi Yamaguchi
Associate Professor
e-mail: hitomiy@ufl.edu

Department of Mechanical and
Aerospace Engineering,
University of Florida,
Gainesville, FL 32611

Force Measurement and Analysis for Magnetic Field–Assisted Finishing

Magnetic field–assisted finishing (MAF) is used to polish free-form surfaces. The material removal mechanism can be described as a flexible "magnetic brush" that consists of ferromagnetic particles and abrasives that arrange themselves in the working gap between the magnet and the workpiece. Relative motion between the brush and the workpiece causes microcutting and improves surface finish. In this study, the contributions of the magnetic and polishing force components to the total force were evaluated. The effect of varying the polishing conditions, such as the working gap and the size of the ferromagnetic iron particles, on polishing forces, surface roughness, and material removal rate was also analyzed. It was observed that the polishing forces varied considerably with working gap. Also, the iron particle size was found to have a strong relation to the rate at which the surface roughness improved. Surface roughness values of 2–3 nm were achieved. [DOI: 10.1115/1.4023723]

1 Introduction

In magnetic field–assisted finishing (MAF), a magnetic field is used to maneuver a flexible "magnetic brush" (composed of ferromagnetic particles and abrasives and formed by the magnetic field) over the surface to be polished. The relative motion between the brush and the surface can be obtained either by rotating the brush, moving the sample, or both. The brush can consist of either: (1) sintered particles, where the ferromagnetic and abrasive particles (e.g., SiC, Al_2O_3, CBN, and diamond) are sintered together to form a ferromagnetic conglomerate or (2) separate abrasive and ferromagnetic particles. For the latter case, the abrasives are held between and within the magnetic chains (brush) that are formed. A lubricant can also be used to aid in holding the abrasive particles within the flexible brush. Figure 1 provides a schematic of the material removal process.

Shinmura et al. [1] first described the MAF process; they used diamond-coated magnetic abrasives manipulated by a magnetic field to finishing cylindrical components. Fox et al. [2] also performed polishing on rollers and studied the effects of slurry type, lubricant, flux density, rotational speed, and vibration. Jain et al. [3] used a pulsed magnetic field to stir the magnetic abrasive slurry and found improved rates of material removal. Yamaguchi and Shinmura [4] used magnetic finishing techniques to polish internal surfaces of tubes. Jain [5] conducted an extensive study of micro/nano MAF and explored the material removal mechanism.

Jayswal et al. [6] developed a numerical technique to simulate the material removal mechanism during MAF and predict the changes in surface roughness. Mori et al. [7] used an energy method to explain the formation of the magnetic abrasive brush and developed a model for polishing forces based on the number of abrasive particles in contact with the surface. Singh et al. [8] employed design of experiments and response surface analysis techniques to develop a model for changes in surface roughness. The parameters considered were working gap, flux density, rotational speed, and abrasive size.

In this study, the forces during magnetic field–assisted polishing were examined. The measured forces were divided into forces due to polishing effects and forces due to magnetic effects. A method to identify and isolate the different elements of the force signal was established. The effect of varying the iron particle sizes and the working gap on polishing forces and surface roughness was examined. The paper is arranged as follows. Section 2 covers the different experimental procedures and analysis techniques used to identify the polishing forces, surface roughness, and material removal rate. The experimental results are presented in Sec. 3. Observations and conclusions are reported in Sec. 4.

2 Experimental Setup and Procedure

In this study, a neodymium permanent magnet (12.7 mm diameter, 12.7 mm length) was used to produce the magnetic field. The magnetic brush was composed of iron particles of different sizes

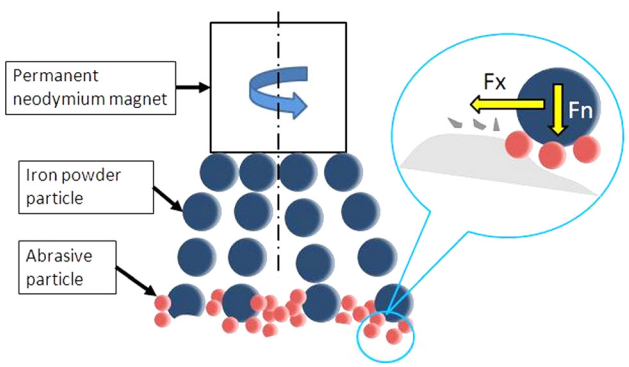

Fig. 1 MAF process (the normal, F_n, and lateral, F_x, force components are identified)

Contributed by the Manufacturing Engineering Division of ASME for publication in the JOURNAL OF MANUFACTURING SCIENCE AND ENGINEERING. Manuscript received August 24, 2012; final manuscript received February 7, 2013; published online July 17, 2013. Assoc. Editor: Y. B. Guo.

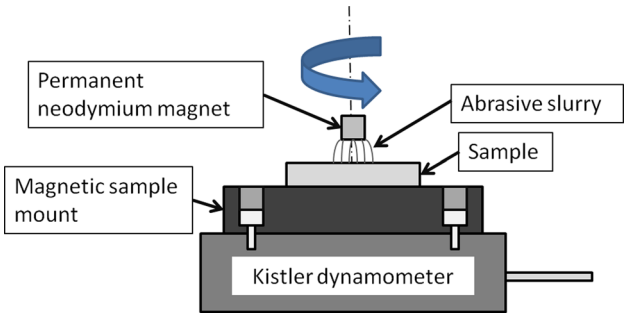

Fig. 2 Schematic of experimental setup

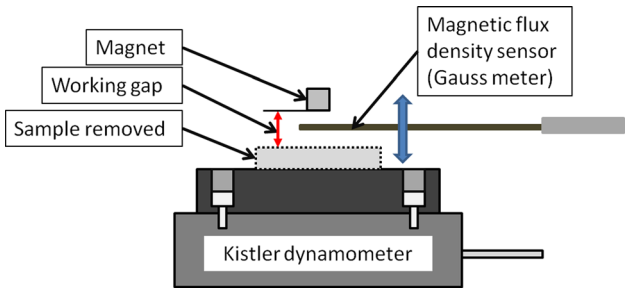

Fig. 3 Schematic of experimental setup for measuring magnetic flux density

Table 1 Polishing conditions (iron powder size)

	PC1	PC2	PC3	PC4
Abrasive diameter (μm)	<0.25	<0.25	<0.25	<0.25
Abrasive amount (mg)	30	30	30	30
Iron powder diameter (μm)	5	44	149	297
Iron powder amount (mg)	300	300	300	300
Lubricant (ml)	0.2	0.2	0.2	0.2
Working gap (mm)	1.5	1.5	1.5	1.5

Table 2 Polishing conditions (working gap size)

	PC5	PC6	PC7	PC8
Abrasive diameter (μm)	<0.25	<0.25	<0.25	<0.25
Abrasive amount (mg)	20	40	60	80
Iron powder diameter (μm)	149	149	149	149
Iron powder amount (mg)	200	400	600	800
Lubricant (ml)	0.13	0.26	0.39	0.52
Working gap (mm)	1	2	3	4

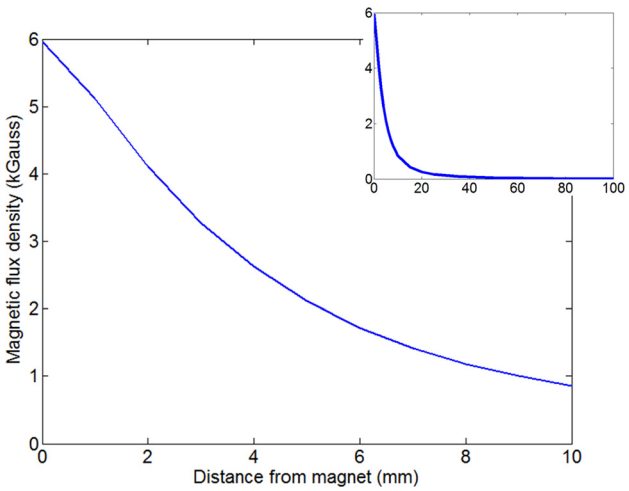

Fig. 4 Magnetic flux density for magnet only

and diamond abrasive. In MAF, the iron particles trap and push the abrasive particles into the workpiece surface, causing material removal. For this work, the relative motion was achieved by rotating the magnet about a vertical axis and translating it parallel to the workpiece surface in horizontal orientation. This ensured that the nonmagnetic diamond abrasive particles were held at the workpiece surface by gravity.

Figure 2 displays a schematic of the experimental setup. The sample (304 stainless steel, 2 mm thick) was mounted using an epoxy resin on a ferromagnetic mount. The ferromagnetic mount provided a path to complete the magnetic circuit. This intensified the magnetic flux density in the working gap between the magnet and the sample and increased the force experienced by the particles in the brush. The sample-mount combination was attached to a three-axis piezoelectric force dynamometer (Kistler 9256C1, 2 mN force resolution). The entire assembly was mounted on the table of a computer numerically-controlled milling machine. The magnet was held in the spindle using a custom holder. The force data was recorded at 300 Hz using a National Instruments data acquisition system and processed in LabView.

In order to conduct a comparative study, the initial surface roughness of all the samples needed to be similar in order to compare the performance of the different polishing conditions. This was achieved by purchasing polished samples and roughening the surface in a controlled and consistent manner using nylon mesh abrasive pads. The samples were measured before MAF to ensure that the initial roughness of all the samples were within a small range (70–90 nm surface area roughness (S_a)).

Polishing tests were completed under several different polishing conditions (PC). The effect of varying the gap size and iron particle size on surface roughness and polishing forces was investigated. The polishing conditions are defined in Tables 1 and 2 (PC1–PC8). For all trials, the spindle speed was 500 rpm and the translational velocity was 100 mm/min. A soluble-type barrel finishing compound (*p*H 9.5, 755 mPa-s at 30 °C) lubricant was used. Diamond was used as the abrasive particles.

2.1 Magnetic Flux Density Measurement. The magnetic flux density in the working gap between the magnetic and sample depends on the strength of the magnet and magnetic permeability of the objects in close proximity. A Gauss meter was used to measure the magnetic flux density in the gap (see Fig. 3). For a given gap, the flux density variation between the magnet and the sample surface was obtained by performing measurements at multiple vertical locations. In order to insert the Gauss meter into the working gap, however, the sample needed to be removed. Since the permeability of 304 stainless steel is negligible (under cold worked conditions, it does become slightly ferromagnetic), the effect of removing the sample on the flux density was considered negligible.

First, the flux density was measured as a function of the distance from the magnet pole with the sample mount removed. Figure 4 shows the measured flux density as a function of distance from the magnet (the inset shows that the flux density asymptotically reduces to zero as the distance increases). Further tests were completed to examine the variation in flux density for different working gaps but with the sample mount in place (see Fig. 5). It is evident that, as the gap size decreases, the flux density in the gap increases. Also, the variation of the flux density (the slope) is lower than for the case when the sample mount was removed. This indicates that the sample mount does indeed provide a path for completion of the magnetic circuit, thereby strengthening the magnetic field in the working gap between the magnet and the sample.

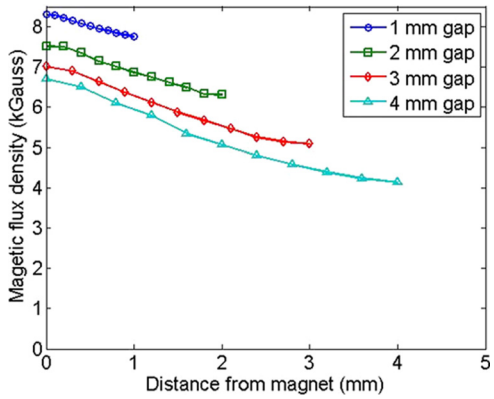

Fig. 5 Magnetic flux density with sample mount

2.2 Polishing Forces Measurement. The polishing forces can be divided into the normal and lateral components. The normal force components act normal to the workpiece surface along the axis of rotation of the permanent magnet, while the lateral forces act tangential to the workpiece surface. The two components were studied independently.

2.2.1 Normal Polishing Forces. The MAF forces can be divided into two categories: (1) magnetic field effects and (2) interactions between the brush and sample due to direct contact or the polishing effect. When studying the forces for different polishing conditions, it is important to accurately separate the two components. The polishing cycle consisted of several steps. First, the magnet was placed in a retracted position, where the effect of the magnetic field on the sample mount was negligible. The piezoelectric dynamometer was reset at this position to give zero force in all directions. The magnet was then advanced toward the sample until the prescribed working gap was reached. The magnet was held at that position for a short period, after which rotation and simultaneous back and forth translation began. After completing the desired number of translations, the rotation was stopped. The magnet was then retracted to its original position.

As noted earlier, in order to accurately isolate the polishing forces from the magnetic forces in the normal force, F_n, it was necessary to identify the force component due to magnetic effects alone. The magnetic forces exist mainly in the normal direction along the axis of the magnet. The symmetry that exists in the two orthogonal directions nullifies the magnetic effects and only polishing forces are measured. The magnetic effects can be divided into three categories.

(i) Effect of sample mount. As the magnet advances towards the sample, it exerts an attractive pull on the ferromagnetic sample mount towards the magnet. This attractive force is observed as a negative normal force (based on the dynamometer orientation). This component is the primary contributor to the magnetic effect.

(ii) Effect of magnetic slurry. The magnetic slurry, when added, acts as an extension of the magnet and produces an additional pull, which is observed as an additional negative normal force.

(iii) Effect of sample magnetism. For a magnetic sample, the magnet exerts a pull on the sample as well. This is also a negative normal force. In this study, this effect was negligible for the 304 stainless steel sample.

In order to identify each of the individual magnetic effects, it was necessary to perform a series of experiments. Using the test results, it was possible to determine the reference level with respect to which the polishing forces could be determined (i.e., the polishing forces could then be isolated from the magnetic effects). These are listed below.

Table 3 Magnetic field effects

	F_{sm} (N)	F_{sl} (N)	F_{sa} (N)	Reference (N)
PC1	16.06	2.14	0.20	−18.40
PC2	16.06	2.04	0.20	−18.30
PC3	16.06	1.83	0.20	−18.09
PC4	16.06	1.28	0.20	−17.54
PC5	19.08	1.74	0.28	−21.10
PC6	13.19	2.55	0.18	−15.92
PC7	9.43	2.14	0.12	−11.69
PC8	6.93	1.94	0.08	−8.96

(i) No sample, no slurry. The polishing cycle was completed with no sample or slurry. This enabled the pull of the magnet on the sample mount to be isolated.

(ii) No sample, slurry. The polishing cycle was completed without the sample but with the slurry. There was still no polishing, because the slurry did not make contact with the sample mount. This test enabled the effect of the slurry on the normal force to be identified.

(iii) Sample, no slurry. The polishing cycle was completed with the sample but without the slurry. There was therefore no polishing. This test enabled the extra pull due to the sample to be determined.

The individual effects were then identified using the following relationships:

Effect of sample mount: $F_{sm} = -F_{n(\text{no sample, no slurry})}$
Effect of slurry: $F_{sl} = F_{n(\text{no sample, slurry})} - F_{n(\text{no sample, no slurry})}$
Effect of sample: $F_{sa} = F_{n(\text{sample, no slurry})} - F_{n(\text{no sample, no slurry})}$

The reference was then computed using the following relationship. Table 3 lists the magnetic field effects obtained for all eight polishing conditions.

$$\text{Reference} = -F_{sm} - F_{sl} - F_{sa}$$

To determine the polishing forces, the polishing cycle was then completed with both the sample and the slurry present. This ensured contact between the slurry and sample and polishing occurred. The normal polishing forces were then computed with respect to the reference.

Normal polishing force: $F_{npol} = F_{n(\text{sample, slurry})} - \text{Reference}$

Figure 6 displays all tests superimposed for PC1. Each individual effect can be identified in the polishing section of the cycle. Figure 7 shows a magnified section of the relevant region where all the various effects have been identified. Other sections of

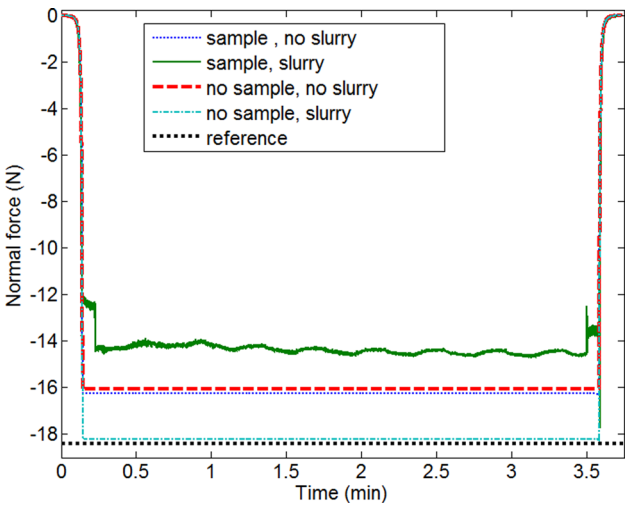

Fig. 6 Normal force measurement (PC1)

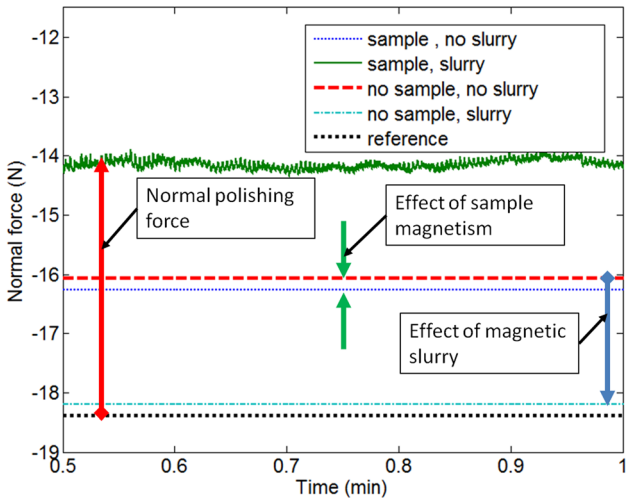

Fig. 7 Normal force effects (PC1)

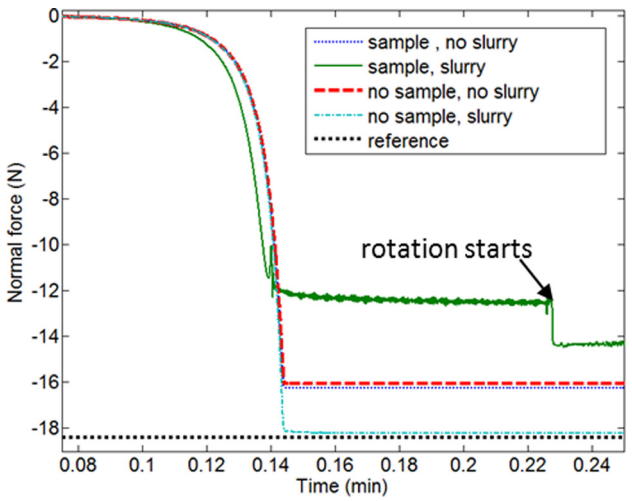

Fig. 8 Normal force (approach) (PC1)

the polishing profile also provide relevant information. Figure 8 shows the magnet approach. As the magnet moves towards the sample, the pull of the magnet on the sample produces a negative normal force. However, as soon as contact is made between the slurry and sample, there is a sudden increase in normal force. This increase is, however, not sustained and quickly reduces to a lower value. This would suggest that there is a realignment of particles in the magnetic brush due to the pressure between the brush and sample. There is a similar drop in force when rotation first begins. This is believed to be due to the centrifugal forces that act on the particles and again leads to a brush realignment and a release of downward pressure on the sample surface.

Figure 9 shows the end of the cycle. When rotation stops, there is an increase in normal force on the sample. This is the opposite of the effect that was witnessed when rotation started. Also, when retraction of the magnet back to its original position begins, there is a negative spike in normal force.

2.2.2 Lateral Polishing Forces. Since the setup is symmetric in the horizontal direction, any magnetic effects are nullified and the dynamometer force in the lateral directions is solely due to polishing effects. However, in order to observe lateral polishing forces, it is necessary that the particles in the brush be translated in addition to rotating. The velocity of each individual particle in the brush is then the sum of its rotational component (due to magnet rotation) and translational component (see Fig. 10).

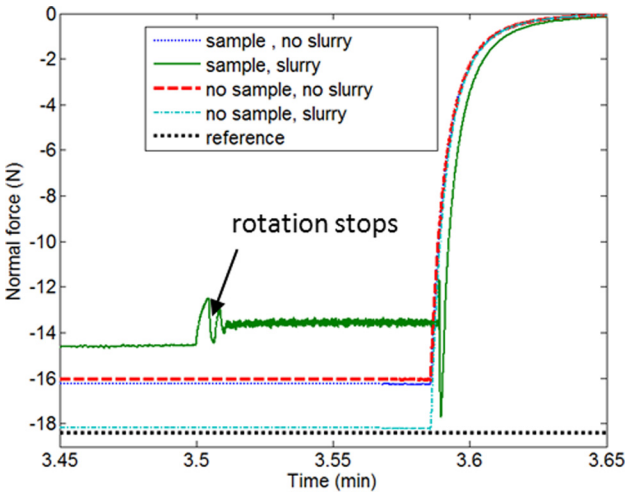

Fig. 9 Normal force (retract) (PC1)

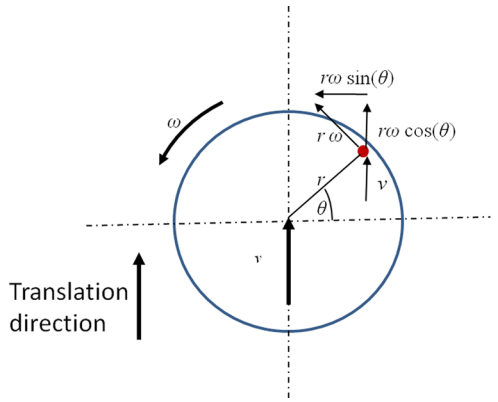

Fig. 10 Velocity components of abrasive particle

The velocity components in the x and y (translation) directions, v_x and v_y, are defined as follows, where v is the translation velocity, r is the radial distance of the particle from the rotating axis, and θ is the angular orientation of the particle.

$$v_x = r\omega \sin(\theta) \quad v_y = v + r\omega \cos(\theta)$$

In most cases, the rotational component is much higher than the translational component, and the different particles in the brush cancel each other and produce near zero net lateral forces. Figures 11(*a*)–11(*c*) show the velocity vectors for the individual particles in the brush at different translational velocities for a fixed rotational speed of 500 rpm. As the translational velocity increases, the number of particles with velocity components in the translation direction also grows.

As a result of the cancelling effect at low translation speeds, the lateral polishing forces cannot be measured simultaneously with normal polishing forces. In order to measure lateral forces, a different polishing cycle was employed. The cycle again consisted of multiple steps. First, the magnet approached the sample from a distance where the magnetic effects were negligible. Once the prescribed working gap was achieved, the magnet was rotated for a brief period (2 seconds). This was necessary to evenly distribute the magnetic slurry below the magnet. The rotation was then stopped and the magnet was translated back and forth for a selected number of cycles. The magnet was then retracted to its original position. The direction of the force measured by the dynamometer naturally changed with the reversal in the translation direction. The lateral polishing force was then defined as the

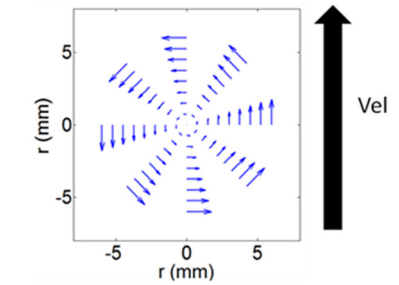

a) Vel = 0 mm/min

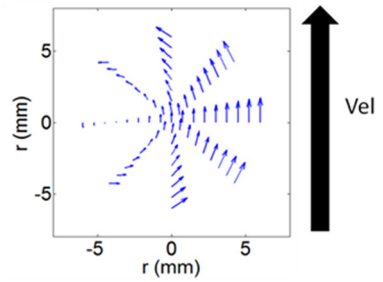

b) Vel = 13000 mm/min

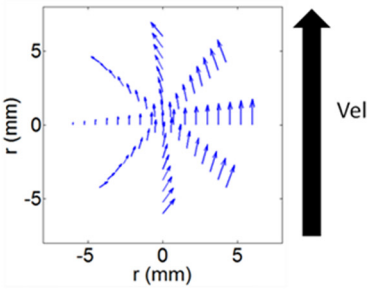

c) Vel = 24000 mm/min

Fig. 11 Velocity vector plot for particles in the brush

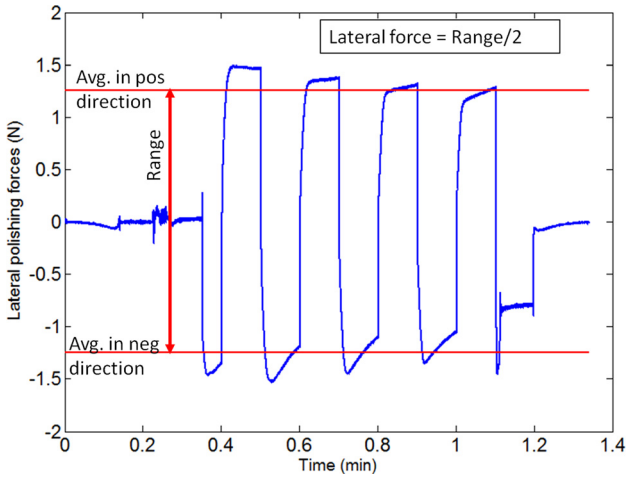

Fig. 12 Lateral force measurement (PC1)

average force from the two translation directions. Figure 12 displays the lateral force measurements for PC1.

2.3 Surface Roughness Measurement. The surface roughness of the samples was measured using a Zygo NewView coherence scanning interferometer (CSI). A 5X Michelson interferometer objective was used for the measurements, which were

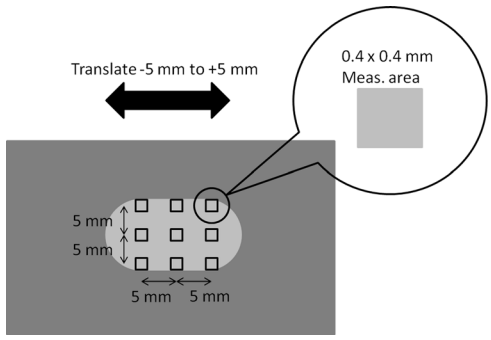

Fig. 13 Schematic of surface roughness measurement locations

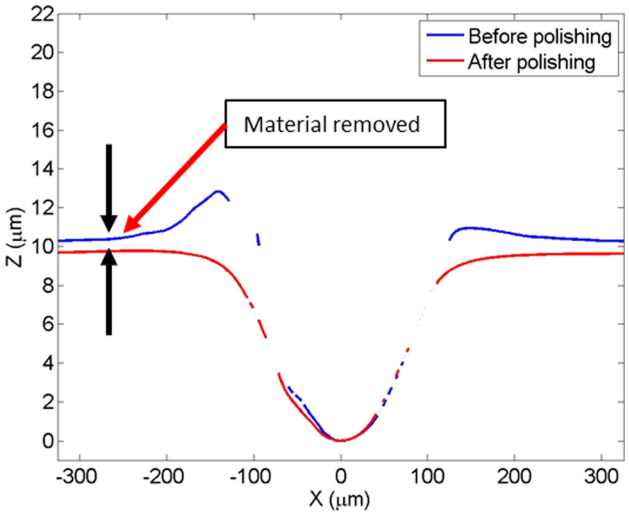

Fig. 14 Cross section of dimple (PC3)

performed after each polishing trial. Area surface roughness (S_a) values were obtained at nine different locations. The S_a value was determined after wavelength filtering using a bandpass filter with low frequency cutoff wavelength of 80 μm and a high frequency cutoff wavelength of 3.31 μm; the low frequency wavelength was 1/5th of the side of the measured area as per ISO 4288 specifications. A fixture was used to accurately relocate the sample with respect to the CSI objective so that the same spot could be measured after each polishing trial. Figure 13 identifies the polished area and the locations at which surface roughness measurements were completed. The samples were prepared as described previously.

2.4 Material Removal Rate Measurement. The effect of iron particle size on the material removal rate (MRR) for magnetic field–assisted finishing was analyzed. The material removed was determined by imaging the sample surface on the CSI before and after polishing. A Zygo ZeGage CSI with a 5X Michelson interferometer objective was used in this case. A set of dimples were created on the sample surface using a spherical indenter. The spherical indenter ensured low slopes at the bottom of the indent, which made it possible to image the bottom of the indent. These indents were imaged on the CSI to measure the depth of the indent. The bottom of the indent was set as the reference surface with respect to which the material removal rate was then determined. It was assumed that there is no material removal at the bottom of the dimple. The MRR, measured change in surface height per unit time (μm/min), is measured from the bottom of the dimple. Figure 14 shows the cross section of the dimple before

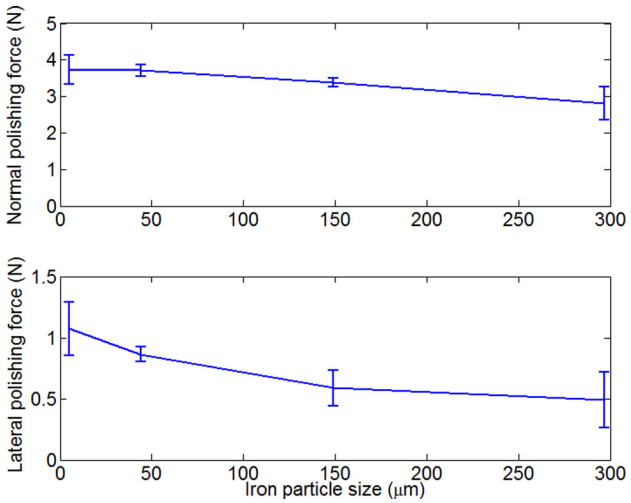

Fig. 15 Polishing force measurements for varying iron particle size (PC1–PC4)

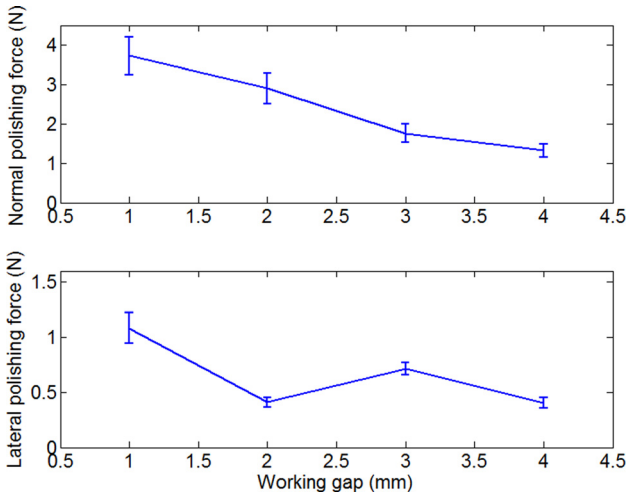

Fig. 16 Polishing force measurements for varying working gap size (PC5–PC8)

and after polishing. Polishing was done for 10 min under condition PC3.

3 Experimental Results

Polishing tests were conducted under a number of different polishing conditions, as defined in Tables 1 and 2.

3.1 Polishing Forces. The polishing forces were measured using the dynamometer, as previously described. The results for the different iron particle sizes and the different working gaps were treated independently.

3.1.1 Varying Iron Particle Size. The iron particle size was varied to examine the effect on polishing force. Four different particle sizes were considered: 5, 44, 149, and 297 μm. All the other parameters were kept constant. Figure 15 displays the corresponding normal and lateral polishing forces, where the error bars represent ± 1 standard deviation obtained from multiple repetitions. The normal force magnitude decreases slightly as the iron particle size increases. This result is counterintuitive, since a larger iron particle would be expected to experience higher forces in the magnetic field. However, the dynamometer does not measure the individual force exerted by each particle but instead

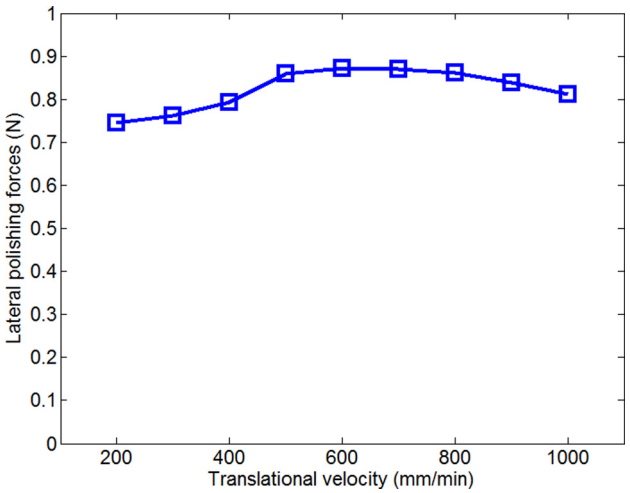

Fig. 17 Effect of velocity on lateral force (PC3)

measures the downward force applied by the entire magnetic brush. It is proposed that the smaller iron particles enable the formation of a more even brush, which causes a larger number of particles to be in contact with the sample. Therefore, although the smaller iron particles may experience smaller magnetic field forces individually, on the whole, they apply more attractive force between the magnet and sample, resulting in a higher normal force measurement. This same effect is also seen in the lateral force measurement.

3.1.2 Varying Working Gap Size. Tests were also completed to examine the effect of working gap size on polishing force and surface roughness. Figure 17 displays the normal and lateral forces obtained at working gaps of 1, 2, 3, and 4 mm. The polishing conditions are defined in Table 2. Note that the mass of the iron particles in the slurry was maintained proportional to the working gap to ensure the same density of slurry in the gap in each case (for a 1 mm gap, the iron particle mass was 200 mg; for a 2 mm gap, the mass was 400 mg, etc.).

Figure 16 shows that the normal polishing force has a strong dependence on the working gap. This is because the flux density decreases as the working gap increases (Fig. 5). The lateral forces are also inversely related to the working gap. All these polishing conditions produced a rapid improvement in surface roughness, so only a single polishing trial was completed. The error bars represent ± 1 standard deviation in force measurement during the single cycle.

3.1.3 Effect of Translation Velocity of Lateral Forces. Lateral forces were measured at several different translation speeds to study the effect of speed on the lateral force magnitude. It was found that translation speed had little impact on lateral force. Figure 17 shows a plot of lateral forces versus translational speeds (PC3).

3.2 Surface Roughness Results. The surface roughness was measured using the Zygo NewView CSI, as earlier described. The results for the different iron particle sizes and the different working gaps are treated independently.

3.2.1 Varying Iron Particle Size. Figure 18 shows the variation of the mean surface roughness values for different iron particle sizes after each polishing trial. The error bars indicate ± 1 standard deviation for the nine measurement locations shown in Fig. 13. This plot clearly shows that the brushes with smaller iron particles produced little to no improvement in the surface roughness, despite exerting larger normal and lateral forces on the sample (Fig. 15). There was a rapid improvement in surface roughness with an iron particle size of 149 μm (PC7) or 297 μm

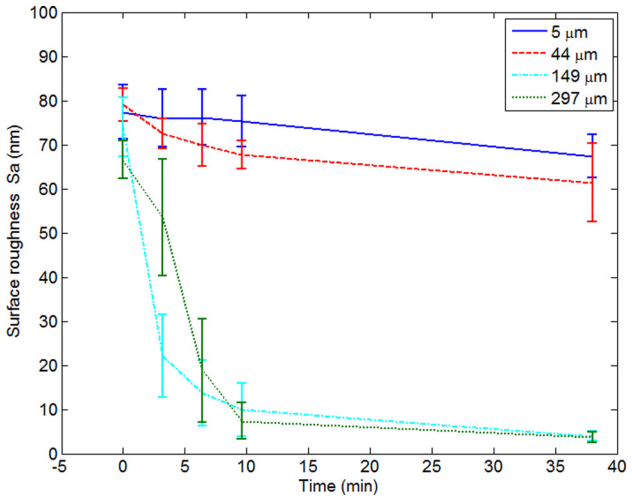

Fig. 18 Surface roughness measurement for varying iron particle size (PC1–PC4)

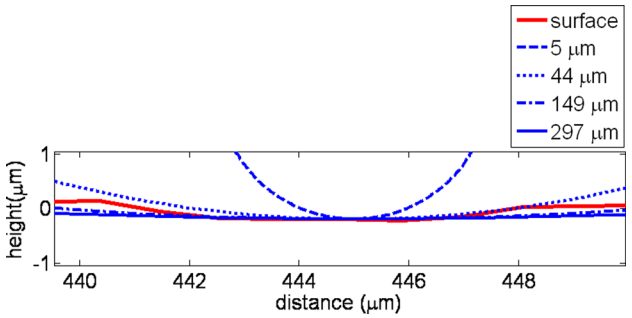

Fig. 19 Surface profile section with schematic of iron particles

(PC8). This is in agreement with the observation made by Jain [5] that there is no material removal when the size of the particle is smaller than the top width of the valley. As the iron particle size increases, particles are prevented from entering the valleys and produce material removal at the peaks. It is also important to note that, although the entire brush might produce larger normal and lateral forces, each individual particle for the smaller-sized iron particles exerts little force on the surface. Thus, the localized polishing force is higher when the iron particle size is greater. This results in a faster improvement in surface roughness.

There is a combination of two factors that dictates whether there is material removal: (1) the size of the iron particles should be larger than the top width of the valleys in the surface and (2) the iron particles must be large enough to impart sufficient force on the abrasive particles to cause material removal. Figure 19 shows a small portion of the surface profile section of the initial surface of the sample along with a schematic representation of the iron particles. The 5 μm and 44 μm iron particles may enter the valleys in the surface, but the 149 μm particle will only cause material removal at the peaks. Note that the particles have been idealized as spheres.

3.2.2 Varying Working Gap Size. Figure 20 shows the time-dependent variation in surface roughness for different working gaps. The results show that, after a polishing time of 6 min, the 1–3 mm gaps produced a similar surface roughness. A larger variation in surface finish improvement may have been observed for a shorter polishing period. For a working gap size of 4 mm (PC8), the final surface roughness was higher. Because the polishing force decreases with increasing gap (especially along the circumference of the brush), there was less material removal

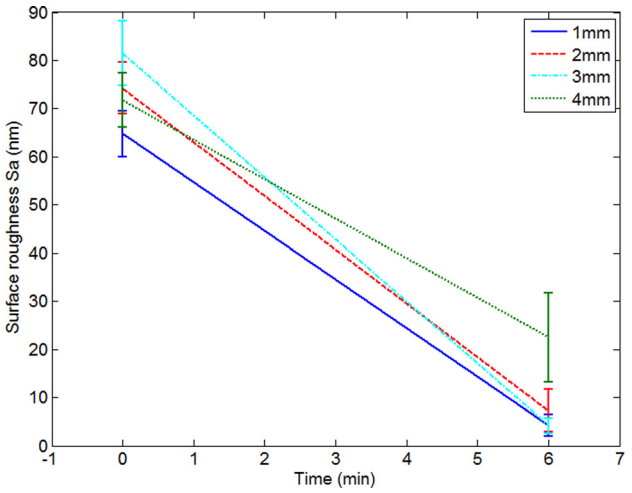

Fig. 20 Surface roughness measurements for varying working gap size (PC1–PC4)

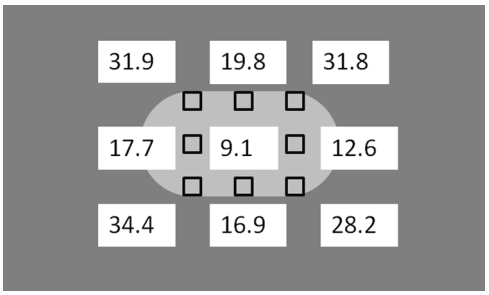

Fig. 21 Surface roughness measurements (S_a in nm) for a working gap of 4 mm (PC8)

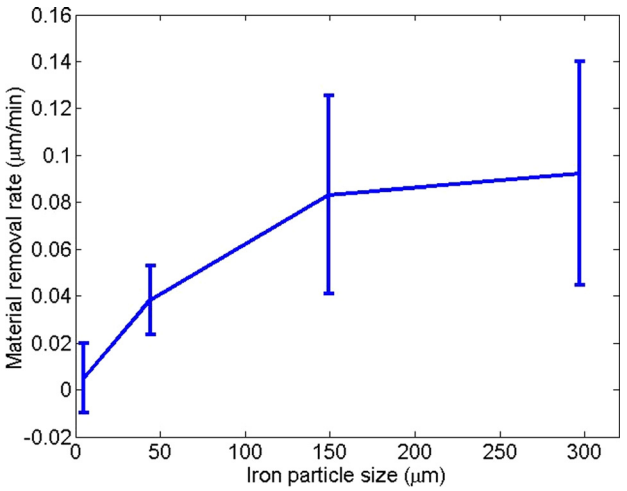

Fig. 22 MRR (μm/min) as a function of IPS (PC1–PC4)

(and polishing) at the periphery, even though there was good material removal in the middle of the brush. Figure 21 shows the surface roughness values at the various locations on the sample after polishing with a working gap of 4 mm (PC8); all values are in nm.

3.3 Material Removal Rate Results. The MRR was measured for trials with different iron particle sizes (PC1–PC4). Polishing was done for 10 min for each trial. The results are plotted in Fig. 22. A Zygo ZeGage CSI was used in this case. The MRR was measured at nine different locations on the sample (as defined in

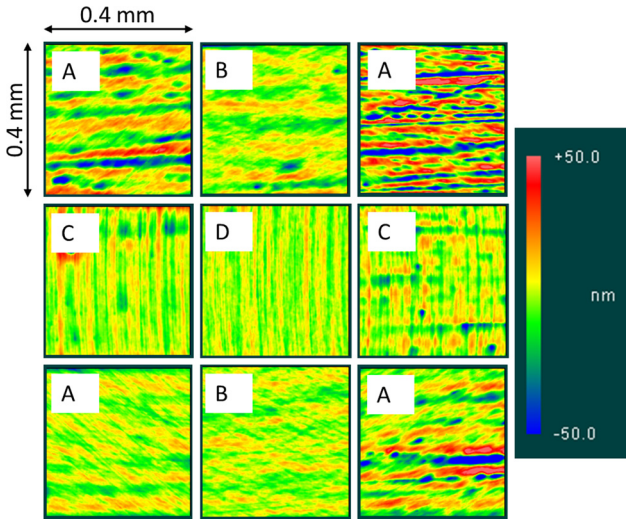

Fig. 23 Direction of lay after polishing (PC3)

Fig. 13). The error bars represent one standard deviation variation in MRR between these nine locations. This result is consistent with the observed change in surface roughness discussed in Sec. 3.2.1, where it was noted that polishing with the smaller iron particle sizes did not result in significant changes in the sample surface.

3.4 Lay Direction. The lay of the polished surface depends on the location with respect to the rotating magnet (rotation and translation tests). Figure 23 shows the CSI measurements for the nine different locations on the sample. This particular set of data corresponds to the surface roughness measurements taken after the third polishing trial with polishing condition PC3 (the point at 9.6 min on the 149 μm line in Fig. 18). The original lay of the surface was horizontal with respect to these measurements (evident from the top right box, where some of the original scratches remain).

The various locations are divided into four groups. The four corners (*a*) only come in contact with the outer periphery of the brush, and they are completely uncovered when the brush has traversed to the opposite end. These locations therefore experience the least improvement in surface roughness. The lay directions are tangential to the brush rotation of the brush and, in this image, are at 45 deg to the window, as expected (note that the top right section has significant residual scratches from the initial surface finish). At the (*b*) locations, the surface is always in contact with the brush. These spots also come in contact with only the outer periphery of the brush. However, as the brush traverses, the asperities at these locations are polished from more than one direction, which, combined with the fact that these locations are in contact with the brush for longer periods, leads to an improvement in the surface roughness over the (*a*) locations. The lay direction forms an "X" at (*b*). At (*c*), the surface comes in contact with the periphery of the brush and also comes directly under the brush when the magnet transverses in that direction. These locations are completely uncovered when the magnet traverses to the opposite end, however. At these locations, the original lay direction is always perpendicular to the velocity of the brush particles. This is the most aggressive angle of attack for material removal and leads to clearly vertical lay directions. At (*d*), which is in the center of the polished area, the surface is always in contact with the brush. At this location, the surface comes in contact with both the periphery and the interior parts of the brush. The instantaneous velocity of the abrasive particles is tangential to the original lay directions. This spot experiences the most aggressive material removal, and the most rapid improvement is surface roughness. The lay direction after polishing is clearly vertical.

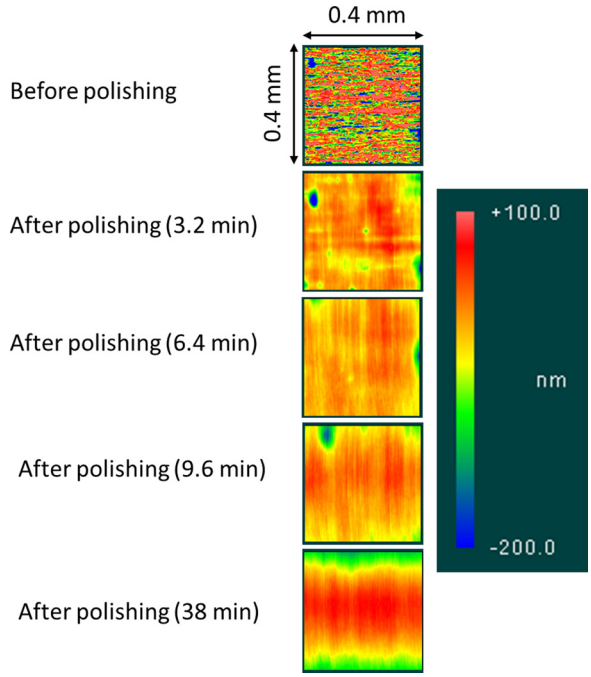

Fig. 24 Variation in surface topography after polishing (PC3)

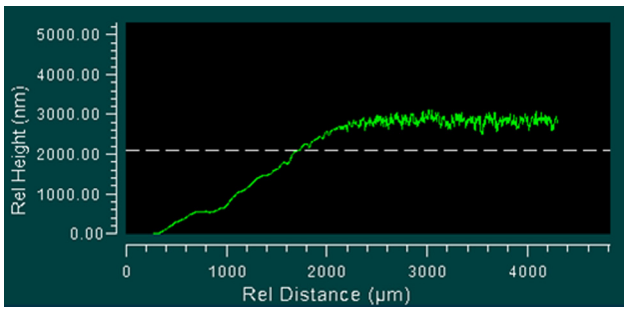

Fig. 25 Cross-sectional view of polished/unpolished interface (PC3)

3.5 Variation in Surface Topography. The variation in surface topography, including waviness, was also investigated. While the previous CSI results were wavelength-filtered to isolate roughness, the filter was removed for this analysis. Figure 24 shows the surface topography of the same location (the center measurement from Fig. 23) after successive polishing trials using PC3. It is seen that the large "divot" in the upper left-hand corner remains through 9.6 min. However, after polishing for a long period of time (38 min), the surface is completely altered and bears little resemblance to the original surface.

A CSI measurement was also completed at the edge of the polished area to identify the amount of material removed (see the cross section in Fig. 25). Approximately 3 μm of material was removed from the original surface (viewed on the right—note that it still exhibits the original roughness prior to polishing). This figure was obtained after 38 min of polishing.

3.6 Variation in Light Intensity. Figure 26 shows light intensity plots obtained using the CSI for the full width of the polished area for four different iron particle sizes. These images were obtained by stitching several measurements together. The total image area is 2 mm $\times$ 15 mm. The unpolished surface is visible at the top and bottom of each image. All polishing trials did produce some visible difference in the surface. However, the PC3

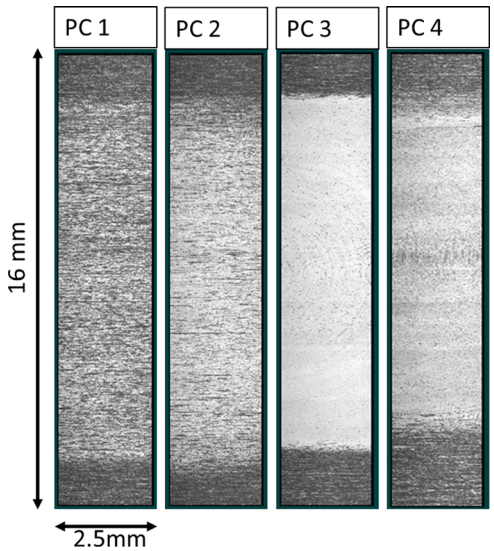

Fig. 26 Light intensity plot of polished area sections (different iron particle sizes) (PC1–PC4)

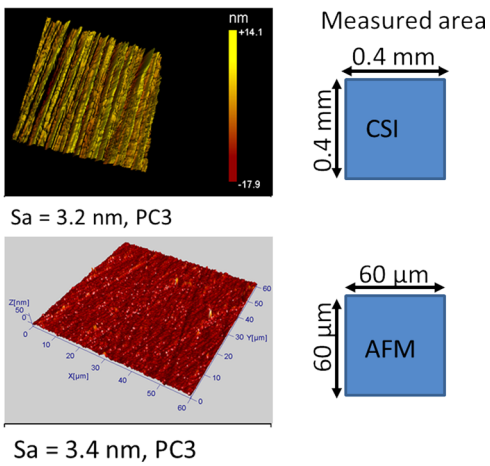

Fig. 27 Comparison of CSI (top) and AFM (bottom) measurements (PC3)

and PC4 surfaces are clearly less rough than the PC1 and PC2 cases.

3.7 Atomic Force Microscope Results. In order to validate the data obtained from the CSI, the results were compared with measurements completed using an atomic force microscope. The scan area for the AFM was $60\,\mu m \times 60\,\mu m$. Figure 27 provides results for PC3. The CSI measurements are on the top. It was found that the results obtained with the AFM were comparable to those obtained using the CSI. Note that the area of the sample being measured was different between the two measurements.

4 Conclusions

In this work, magnetic field assisted finishing (MAF) was used to polish 304 stainless steel samples with ferromagnetic particles and diamond abrasives. A technique for isolating the polishing forces from the magnetic forces was described. The effect of varying the polishing conditions, such as the working gap and the size of the ferromagnetic iron particles, on surface roughness and polishing forces was investigated. A number of conclusions can be drawn based on the experimental results and analysis.

- The addition of a ferromagnetic mount behind the sample serves to aid in completing the magnetic circuit and increases the magnetic flux density in the working gap. This leads to higher polishing forces.
- While measuring MAF polishing forces, it is necessary to isolate the magnetic field effects from the polishing effects.
- The normal and lateral forces were found to have an inverse relationship with both iron particle size and working gap.
- The rate of improvement in surface roughness with polishing time depends on the iron particle size. If the particles are too small, there is little material removal, even after polishing for prolonged periods of time. The rate of improvement in surface roughness is not sensitive to the working gap. However, for larger gaps, the material removal at the periphery of the brush reduces rapidly. The amount of slurry was maintained proportional to the gap size in this study.
- The improvement in surface roughness decays with increased polishing time. Further improvement requires a change in the polishing conditions.
- The translational velocity has almost no effect on the magnitude of lateral polishing force.
- The material removal rate is higher when polishing using larger iron particle sizes.
- The lay of the polished surface is dictated by the path of the magnetic field and the direction of the abrasive particles.
- The final surface topography depends on the polishing time.

Acknowledgment

The authors gratefully acknowledge financial support from the National Science Foundation (Grant No. 0855381).

References

[1] Shinmura, T., Takazawa, K., Hatano, E., Matsunaga, M., and Matsuo, T., 1990, "Study on Magnetic Abrasive Finishing," CIRP Ann., **39**(1), pp. 325–328.
[2] Fox, M., Agrawal, K., Shinmura, T., and Komanduri, R., 1994, "Magnetic Abrasive Finishing of Rollers," CIRP Ann., **43**(1), pp. 181–184.
[3] Jain, V. K., Singh, D. K., and Raghuram, V., 2008, "Analysis of Performance of Pulsating Flexible Magnetic Abrasive Brush (P-FMAB)," Mach. Sci. Technol., **12**(1), pp. 53–76.
[4] Yamaguchi, H., and Shinmura, T., 1999, "Study of the Surface Modification Resulting From an Internal Magnetic Abrasive Finishing Process," Wear, **225–229**, pp. 246–255.
[5] Jain, V. K., 2009, "Magnetic Field Assisted Abrasive Based Micro-/Nano-Finishing," J. Mater. Process. Technol., **209**(20), pp. 6022–6038.
[6] Jayswal, S. C., Jain, V. K., and Dixit, P. M., 2005, "Modeling and Simulation of Magnetic Abrasive Finishing Process," Int. J. Adv. Manuf. Technol., **26**(5–6), pp. 477–490.
[7] Mori, T., Hirota, K., and Kawashima, Y., 2003, "Clarification of Magnetic Abrasive Finishing Mechanism," J. Mater. Process. Technol., **143–144**, pp. 682–686.
[8] Singh, D. K., Jain, V. K., and Raghuram, V., 2009, "Parametric Study of Magnetic Abrasive Finishing Process," J. Mater. Process. Technol., **149**, pp. 22–29.